

# Aging and rejuvenation during elastostatic loading of amorphous alloys

Nikolai V. Priezjev<sup>1,2</sup>

<sup>1</sup>*Department of Mechanical and Materials Engineering,  
Wright State University, Dayton, OH 45435 and*

<sup>2</sup>*National Research University Higher School of Economics, Moscow 101000, Russia*

(Dated: May 3, 2019)

## Abstract

Using molecular dynamics simulations, we investigate the effect of uniaxial elastostatic compression on the potential energy, structural relaxation, and mechanical properties of binary glasses. We consider the three-dimensional Kob-Andersen binary mixture, which was initially cooled from the liquid state to the glass phase with a slow rate at zero pressure. The glass was then loaded with a static stress at the annealing temperature during extended time intervals. It is found that the static stress below the yielding point induces large-scale plastic deformation and significant rejuvenation when the annealing temperature is smaller than a fraction of the glass transition temperature. By contrast, aging effects become dominant at sufficiently small values of the static stress and higher annealing temperatures. The mechanical tests after the elastostatic compression have shown that both the elastic modulus and the yield stress decrease in rejuvenated samples, while the opposite trend was observed for relaxed glasses. These results might be useful for the thermomechanical processing of metallic glasses with optimized mechanical properties.

Keywords: metallic glasses, deformation, mechanical treatment, yield stress, molecular dynamics simulations

## I. INTRODUCTION

The development and implementation of novel processing techniques for metallic glasses in order to optimize their mechanical properties is important for numerous structural and biomedical applications [1]. It is well known however that in contrast to crystalline materials, plastic deformation of metallic glasses is associated with the formation of very localized shear bands, thus preventing their widespread use [1]. In practice, improved mechanical properties can be achieved by relocating metallic glasses to higher potential energy states using various thermal and mechanical treatments, such as cold rolling, shot peening, high pressure torsion, ion irradiation, and, more recently, cryogenic thermal cycling [2, 3]. Alternatively, in cases when the shape change due to flow is not important, higher energy states can be attained by reheating amorphous alloys above the glass transition temperature followed by suitably fast cooling back to the glass state [4–7]. Somewhat unexpectedly, a convenient and efficient method to enhance the potential energy of a glass is to simply apply a static stress in the elastic range and let the system accumulate irreversible structural transformations [8–16]. Thus, it was demonstrated experimentally that the elastostatic compression of Zr-based bulk metallic glasses leads to a significant increase in enthalpy, which is comparable with the states produced upon very fast quenching from the liquid state or by severe plastic deformation [15]. Furthermore, upon increasing stress, a transition from relaxation to rejuvenation in metallic glasses subjected to elastostatic compression was observed [14]. Despite recent progress, however, the mechanisms of rejuvenation as well as the details of the elastostatic loading protocol required for the maximum energy storage remain not fully understood.

In recent years, atomistic simulations were particularly useful in elucidating the relaxation dynamics of amorphous alloys subjected to various deformation protocols including oscillatory shear strain [17–25], constant [26] and periodic [27, 28] elastic stress, as well as thermal cycling [29, 30]. It was originally found that physical aging below the glass transition temperature can be reversed by plastic deformation [31], while the glass becomes effectively overaged when reversibly deformed below yield [32]. Interestingly, the structural relaxation slows down in case of multiple subyield cycles, leading to progressively lower potential energy states as the cycle number increases [20, 22, 23, 28]. On the other hand, the yielding transition occurs after a certain number of transient cycles if the strain amplitude is sufficiently large, and the increase in the potential energy is caused by the formation of

a system-spanning shear band [20, 21, 23]. However, the precise control of the degree of relaxation or rejuvenation during processing of metallic glasses remains a challenging task due to the vast parameter space involved in loading protocols.

In this paper, molecular dynamics simulations are performed to examine the effect of elastostatic loading on the potential energy states and mechanical properties of an amorphous alloy. After slow initial cooling to a temperature well below the glass transition temperature, the binary glass is loaded with a static stress in the elastic range at the annealing temperature for extended periods of time. It will be shown that aging effects are predominant at sufficiently low values of the applied stress when the annealing temperature is greater than approximately half  $T_g$ . By contrast, high compressive stress (below yield) induces large-scale plastic deformation and significant rejuvenation at low annealing temperatures. As a result of the treatment, aged/rejuvenated samples exhibit higher/lower yield stress and elastic modulus during strain-controlled compression.

This paper is structured as follows. The parameters of the molecular dynamics simulation model and the details of the loading protocol are given in the next section. The dependence of the potential energy, elastic modulus, and yield stress on the annealing time, temperature, and static stress, as well as spatial configurations of mobile atoms are presented in section III. The results are briefly summarized in the last section.

## II. MOLECULAR DYNAMICS SIMULATIONS

The amorphous alloy is modeled using the Lennard-Jones (LJ) binary (80:20) mixture first introduced over twenty years ago by Kob and Andersen (KA) [33]. The LJ parameters of the KA model is similar to the parametrization proposed by Weber and Stillinger to simulate the amorphous metal alloy Ni<sub>80</sub>P<sub>20</sub> [34]. In the KA model, any two atoms of types  $\alpha, \beta = A, B$  interact via the truncated LJ potential:

$$V_{\alpha\beta}(r) = 4\varepsilon_{\alpha\beta} \left[ \left( \frac{\sigma_{\alpha\beta}}{r} \right)^{12} - \left( \frac{\sigma_{\alpha\beta}}{r} \right)^6 \right], \quad (1)$$

with the parameters:  $\varepsilon_{AA} = 1.0$ ,  $\varepsilon_{AB} = 1.5$ ,  $\varepsilon_{BB} = 0.5$ ,  $\sigma_{AA} = 1.0$ ,  $\sigma_{AB} = 0.8$ ,  $\sigma_{BB} = 0.88$ , and  $m_A = m_B$  [33]. This choice of parameters corresponds to strongly non-additive interaction between atoms  $A$  and  $B$ , which prevents crystallization when the binary mixture is cooled below the glass transition temperature [33]. To reduce the computational demand,

the cutoff radius of the LJ potential is set to  $r_{c,\alpha\beta} = 2.5 \sigma_{\alpha\beta}$  throughout the study. The total number of atoms is  $N = 60\,000$ . The LJ units of length, mass, energy, and time are adopted for all physical quantities as follows:  $\sigma = \sigma_{AA}$ ,  $m = m_A$ ,  $\varepsilon = \varepsilon_{AA}$ , and  $\tau = \sigma \sqrt{m/\varepsilon}$ . All simulations were carried out using the LAMMPS software [35] with the integration time step  $\Delta t_{MD} = 0.005 \tau$ .

The binary glass was first prepared by equilibrating the mixture at the temperature  $T_{LJ} = 1.0 \varepsilon/k_B$  and zero pressure, using periodic boundary conditions. Here,  $k_B$  and  $T_{LJ}$  denote the Boltzmann constant and temperature, respectively. The temperature was controlled via the Nosé-Hoover thermostat [35, 36]. Then, the binary mixture was gradually cooled with the computationally slow rate  $10^{-5} \varepsilon/k_B \tau$  at zero pressure to the reference temperature of  $0.01 \varepsilon/k_B$ . A snapshot of the amorphous alloy at  $T_{LJ} = 0.01 \varepsilon/k_B$  and  $P = 0$  is shown in Fig. 1.

Next, the loading protocol was implemented via heating and at the same time applying the normal stress along the  $\hat{z}$  direction during  $5000 \tau$ . Then, the system was allowed to evolve during the time period  $t_a$  at the annealing temperature  $T_a$  and the static normal stress along the  $\hat{z}$  direction, while the pressure along the  $\hat{x}$  and  $\hat{y}$  directions were set to zero. The last step is the decrease of temperature and normal stress to the reference state, *i.e.*,  $T_{LJ} = 0.01 \varepsilon/k_B$  and  $P = 0$  in all three dimensions. Thus, the control parameters of the elastostatic loading process include the annealing temperature, the normal stress, and the annealing time. During each step of the process, the temperature, stress components, potential energy, and system dimensions were saved for further analysis. In addition, the mechanical properties were probed by imposing the compressive strain along the  $\hat{x}$  direction with the constant rate  $\dot{\varepsilon}_{xx} = 10^{-5} \tau^{-1}$  at  $T_{LJ} = 0.01 \varepsilon/k_B$  and  $P = 0$ . Due to computational limitations, the simulations were performed for only one realization of disorder.

### III. RESULTS

It is well recognized by now that the structural and mechanical properties of metallic glasses depend sensitively on the rate of cooling from the liquid state [31]. Although in all cases the glass structure is amorphous, more slowly annealed glasses settle down into deeper energy minima and their global yield stress becomes higher [1]. A more subtle characteristic of the quenched glass is a broad distribution of the local yield stresses, whose

peak is displaced to higher values in more slowly annealed glasses [37]. Loosely speaking, a well annealed glass can be viewed as a rigid matrix with randomly embedded soft spots that have relatively low local yield stresses [13]. When a static stress below the global yield is applied, the matrix is elastically deformed but the soft spots are prone to plastic deformation over time, which might lead to rejuvenation and, as a result, to improved plasticity. In what follows, we explore a wide range of parameters, including the annealing temperature, time and static stress, and observe both aging and rejuvenation in well annealed binary glasses.

It was previously shown that the glass transition temperature of the KA binary mixture is  $T_g \approx 0.35 \varepsilon/k_B$ , which was estimated by extrapolating the potential energy from the low and high temperature regions when the system was cooled with the rate  $10^{-5} \varepsilon/k_B \tau$  at zero pressure [7]. In order to determine the values of the stress overshoot at different temperatures, the compressive strain was applied to samples right after cooling from the liquid state, *i.e.*, to untreated samples. The stress-strain curves are presented in Fig. 2 for selected values of  $T_{LJ}$  lower than  $T_g$ . As expected, upon decreasing  $T_{LJ}$ , the peak value of the stress overshoot becomes higher and the corresponding yield strain increases. In the analysis below, the elastic modulus  $E = 60.73 \varepsilon \sigma^{-3}$  and the stress overshoot  $\sigma_Y = 2.61 \varepsilon \sigma^{-3}$ , extracted from the stress-strain curve at  $T_{LJ} = 0.01 \varepsilon/k_B$ , will serve as reference values for comparison with treated samples.

We next describe the elastostatic loading protocol and discuss the choice of parameter values for the static stress, annealing temperature, and the reference state. After the annealing time interval, the glass was always brought to the reference state at  $T_{LJ} = 0.01 \varepsilon/k_B$  and  $P = 0$  to facilitate comparison of the potential energy and mechanical properties. For example, the variation of temperature during the loading process is illustrated in Fig. 3 for the annealing time  $t_a = 10^5 \tau$ . It can be seen that during the first  $5000 \tau$ , the temperature was ramped linearly to  $T_a$  and kept constant during the annealing time  $t_a$ . At the same time, the normal stress,  $\sigma_{zz}$ , increased from zero to a finite value during the first  $5000 \tau$  (not shown) and remained constant during  $t_a$ , while the other stress components  $\sigma_{xx} = \sigma_{yy} = 0$ . After the time interval  $t_a$ , both the temperature and normal stress were reduced back to their values at the reference state ( $T_{LJ} = 0.01 \varepsilon/k_B$  and  $\sigma_{zz} = 0$ ) during  $5000 \tau$ . Once at reference state, the potential energy was computed, and the sample was compressed along the  $\hat{x}$  direction with a constant strain rate to measure the stress response (to be discussed

below).

The dependence of the potential energy as a function of the annealing time is shown in Fig. 4 for the annealing temperatures  $T_a = 0.05 \varepsilon/k_B$ ,  $0.1 \varepsilon/k_B$ ,  $0.2 \varepsilon/k_B$ , and  $0.25 \varepsilon/k_B$ . For each  $T_a$ , the simulations were performed for several values of the static stress,  $\sigma_{zz}$ , smaller than the stress overshoot reported in Fig. 2. Note that the potential energy level before the treatment,  $U = -8.337 \varepsilon$ , is denoted by the dashed lines in Fig. 4. It is readily apparent that the aging effects at  $\sigma_{zz} = 0$  are negligible for  $T_a \leq 0.1 \varepsilon/k_B$ , whereas  $U$  decreases monotonically at higher temperatures  $T_a = 0.2 \varepsilon/k_B$  and  $0.25 \varepsilon/k_B$  during  $t_a = 2.4 \times 10^6 \tau$ .

The influence of the static stress is reflected in the increase of the potential energy with respect to  $U(T_a, t_a)$  at  $\sigma_{zz} = 0$ , as shown in Fig. 4. The most pronounced increase in  $U$  occurs when the static stress is sufficiently close to the yield stress. For example, the most rejuvenated states at  $T_a = 0.1 \varepsilon/k_B$  are obtained when  $\sigma_{zz} = 1.5 \varepsilon \sigma^{-3}$  in Fig. 4 (b), while the peak value of the stress overshoot at  $T_{LJ} = 0.1 \varepsilon/k_B$  in Fig. 2 is about  $1.9 \varepsilon \sigma^{-3}$ . In general, it is difficult to identify a threshold value of the static stress that leads to maximum rejuvenation and at the same time does not cause significant deformation of the simulation domain over time. For instance, when the glass was loaded with  $\sigma_{zz} = 1.2 \varepsilon \sigma^{-3}$  at  $T_a = 0.2 \varepsilon/k_B$ , the system became fully compressed along the  $\hat{z}$  direction after about  $3.5 \times 10^4 \tau$ , despite that the magnitude of the yielding peak is  $\approx 1.43 \varepsilon \sigma^{-3}$  at  $T_{LJ} = 0.2 \varepsilon/k_B$  in Fig. 2. Furthermore, the transition from aging to rejuvenation upon increasing  $\sigma_{zz}$  is seen most clearly at  $T_a = 0.2 \varepsilon/k_B$  in Fig. 4 (c). We finally comment that static loading at  $T_a = 0.25 \varepsilon/k_B$  only reduces the effect of aging but the potential energy remains below the level for the untreated sample, as shown in Fig. 4 (d). Similarly, test runs at the higher annealing temperature  $T_a = 0.3 \varepsilon/k_B$  indicated that  $U$  also decreases over time for any values of the applied static stress (not shown).

The details of the structural relaxation process can be unveiled by analyzing the so-called nonaffine displacements of atoms [38]. In other words, the temporal evolution of the system can be visualized as a sequence of the relative displacements of atoms with respect to their neighbors. More specifically, the nonaffine measure for the  $i$ -th atom is defined by computing the transformation matrix  $\mathbf{J}_i$ , which performs a linear transformation of its

neighboring atoms during the time interval  $\Delta t$  and minimizes the following expression:

$$D^2(t, \Delta t) = \frac{1}{N_i} \sum_{j=1}^{N_i} \left\{ \mathbf{r}_j(t + \Delta t) - \mathbf{r}_i(t + \Delta t) - \mathbf{J}_i [\mathbf{r}_j(t) - \mathbf{r}_i(t)] \right\}^2, \quad (2)$$

where the sum is taken over the atoms within a sphere of radius  $1.5\sigma$  centered at  $\mathbf{r}_i(t)$ . In particular, it was recently shown that the amplitude of nonaffine displacements during oscillatory deformation of amorphous solids is approximately power-law distributed, and most of the atoms undergo reversible displacements after one or several cycles when the strain amplitude is below the yielding point [18, 19]. Furthermore, the formation of shear bands at the yielding transition was readily detected by identifying atoms with relatively large nonaffine displacements (larger than the typical cage size) during one shear cycle in both poorly [23] and well [21] annealed glasses. In general, the nonaffine measure is also an excellent diagnostic of local structural rearrangements during mechanical [22, 23, 28] and thermal [29] annealing processes, when disordered solids gradually evolve towards low potential energy states.

The representative spatial configurations of atoms with relatively large nonaffine measure,  $D^2(0, t_a) > 0.04\sigma^2$ , are displayed in Fig. 5 for  $\sigma_{zz} = 0.5\epsilon\sigma^{-3}$  and in Fig. 6 for  $\sigma_{zz} = 1.5\epsilon\sigma^{-3}$  during loading at  $T_a = 0.1\epsilon/k_B$ . To remind, the analysis of nonaffine displacements between two atomic configurations separated by the time interval  $t_a$  was performed when the system was brought to the reference state at  $T_{LJ} = 0.01\epsilon/k_B$  and  $P = 0$ . Since the typical cage size is  $r_c \approx 0.1\sigma$ , Figs. 5 and 6 only show atoms that left their cages during  $t_a$ , and, therefore, they represent the local plastic deformation of the material. It can be observed in Fig. 5 that mobile atoms are organized into small clusters whose size slightly increases over time, while the net effect of these transformations on the potential energy is negligible [see the data for  $\sigma_{zz} = 0.5\epsilon\sigma^{-3}$  in Fig. 4 (b)]. By contrast, loading at  $T_a = 0.1\epsilon/k_B$  and  $\sigma_{zz} = 1.5\epsilon\sigma^{-3}$  induces extended clusters that become comparable with the system size when  $t_a \gtrsim 10^6\tau$  (see Fig. 6), which leads to significant rejuvenation, as shown in Fig. 4 (b). We comment that despite large-scale structural rearrangements at  $\sigma_{zz} = 1.5\epsilon\sigma^{-3}$ , the net compression along the  $\hat{z}$  direction is relatively small; *i.e.*, from  $L_z = 36.54\sigma$  at  $t_a = 0$  to  $L_z = 36.11\sigma$  at  $t_a = 2.4 \times 10^6\tau$ .

It should be emphasized that there is a crucial difference between rejuvenated states obtained via elastostatic loading and cyclic shear with the strain amplitude above the yield-

ing point. In the latter case, the increase in the potential energy is directly related to the formation of a fluidized shear band [20, 21, 23, 25], while in the former case, the plastic deformation under static stress is distributed more homogeneously in the regions with relatively low local yield stress. The next comment is regarding the structural characteristics at different energy states. It was previously shown that unlike Zr-based metallic glasses, where the icosahedral short-range order is a sensitive indicator of structural changes, the KA binary glass does not contain frequent icosahedral structures, but instead its microscopic structure is rather sensitive to the shape of the pair correlation function of small atoms of type  $B$  [7, 31, 39]. In the recent study on thermal processing of binary glasses, the changes in the potential energy were correlated with the height of the nearest-neighbor peak in the  $BB$  pair correlation function [7]. Since the variation of the potential energy reported in Fig. 4 is comparable with energy changes found in Ref. [7] and the variation of the peak height was relatively small, the structural analysis was not performed in the present study.

We finally report the elastic modulus in Fig. 7 and the peak value of the stress overshoot in Fig. 8 as functions of the annealing time and temperatures  $T_a = 0.05 \varepsilon/k_B$ ,  $0.1 \varepsilon/k_B$ ,  $0.2 \varepsilon/k_B$ , and  $0.25 \varepsilon/k_B$ . In each case, the stress was computed during compression along the  $\hat{x}$  direction with the rate  $\dot{\varepsilon}_{xx} = 10^{-5} \tau^{-1}$  at  $T_{LJ} = 0.01 \varepsilon/k_B$  and  $\sigma_{zz} = \sigma_{yy} = 0$ . Although the data are somewhat scattered, it is evident in Figs. 7 and 8 that aged/rejuvenated glasses exhibit higher/lower values of  $E$  and  $\sigma_Y$ . The most pronounced decrease in the elastic modulus and yield stress occurs for the following parameters of the loading protocol ( $T_a$ ,  $\sigma_{zz}$ ):  $(0.05 \varepsilon/k_B, 1.8 \varepsilon\sigma^{-3})$ ,  $(0.1 \varepsilon/k_B, 1.5 \varepsilon\sigma^{-3})$ , and  $(0.2 \varepsilon/k_B, 1.0 \varepsilon\sigma^{-3})$ . Interestingly, a similar decrease in  $E$  and  $\sigma_Y$  (about 10%) was reported in the recent study where a glass was reheated above  $1.3 T_g$  and then quenched with a rate of about  $10^{-3} \varepsilon/k_B \tau$  to the glass phase [7]. We lastly mention that the increase in  $\sigma_Y$  as a function of  $t_a$  at  $\sigma_{zz} = 0$  shown in Fig. 8(c, d) is consistent with the results of previous studies on the effect of physical aging on the yield stress [40, 41].

#### IV. CONCLUSIONS

In summary, the influence of prolonged elastostatic compression on the potential energy, structural relaxation, and mechanical properties of binary glasses was examined using molecular dynamics simulations. The model glass was represented via the Lennard-Jones binary



mixture, which was initially annealed from the liquid state to the glass phase with a computationally slow rate at zero pressure. During the thermomechanical treatment, the glass was loaded with a compressive stress and annealed at a constant temperature. It was found that the static stress below the yield stress induces significant rejuvenation due to large-scale plastic deformation. In contrast, at sufficiently low stress levels, aging becomes dominant when the annealing temperature is greater than about half  $T_g$ . After the elastostatic loading, both the elastic modulus and the yield stress were found to decrease in rejuvenated glasses, while the opposite trend was reported for aged samples.

### Acknowledgments

Financial support from the National Science Foundation (CNS-1531923) is gratefully acknowledged. The article was prepared within the framework of the HSE University Basic Research Program and funded in part by the Russian Academic Excellence Project ‘5-100’. The molecular dynamics simulations were performed using the LAMMPS software developed at Sandia National Laboratories [35]. The numerical simulations were performed at Wright State University’s Computing Facility and the Ohio Supercomputer Center.

- 
- [1] Y. Sun, A. Concustell, and A. L. Greer, Thermomechanical processing of metallic glasses: extending the range of the glassy state, *Nat. Rev. Mater.* **1**, 16039 (2016).
  - [2] S. V. Ketov, Y. H. Sun, S. Nachum, Z. Lu, A. Checchi, A. R. Beraldin, H. Y. Bai, W. H. Wang, D. V. Louzguine-Luzgin, M. A. Carpenter, and A. L. Greer, Rejuvenation of metallic glasses by non-affine thermal strain, *Nature* **524**, 200 (2015).
  - [3] W. Guo, J. Saida, M. Zhao, S. Lu, and S. Wu, Rejuvenation of Zr-based bulk metallic glass matrix composite upon deep cryogenic cycling, *Materials Letters* **247**, 135 (2019).
  - [4] M. Wakeda, J. Saida, J. Li, and S. Ogata, Controlled rejuvenation of amorphous metals with thermal processing, *Sci. Rep.* **5**, 10545 (2015).
  - [5] S. Kuchemann, P. M. Derlet, C. Liu, D. Rosenthal, G. Sparks, W. S. Larson, and R. Maass, Energy Storage in Metallic Glasses via Flash Annealing, *Adv. Funct. Mater.* **28**, 1805385 (2018).

- [6] M. Wang, H. Liu, J. Mo, Y. Zhang, Z. Chen, C. Yin, and W. Yang, Thermal-pressure effects on energy state of metallic glass  $\text{Cu}_{50}\text{Zr}_{50}$ , *Comput. Mater. Sci.* **155**, 493 (2018).
- [7] N. V. Priezjev, Atomistic modeling of heat treatment processes for tuning the mechanical properties of disordered solids, *J. Non-Cryst. Solids* (2019). 10.1016/j.jnoncrysol.2019.03.031
- [8] K.-W. Park, C.-M. Lee, M. Wakeda, Y. Shibutani, M. L. Falk, and J.-C. Lee, Elastostatically induced structural disordering in amorphous alloys, *Acta Materialia* **56**, 5440 (2008).
- [9] C.-M. Lee, K.-W. Park, B.-J. Lee, Y. Shibutani and J.-C. Lee, Structural disordering of amorphous alloys: A molecular dynamics analysis, *Scripta Materialia* **61**, 911 (2009).
- [10] Y. Tong, W. Dmowski, Y. Yokoyama, G. Wang, P. K. Liaw, and T. Egami, Recovering compressive plasticity of bulk metallic glasses by high-temperature creep, *Scripta Materialia* **69** 570 (2013).
- [11] Y. M. Wang, M. Zhang and L. Liu, Mechanical annealing in the homogeneous deformation of bulk metallic glass under elastostatic compression, *Scripta Materialia* **102**, 67 (2015).
- [12] L. Z. Zhao, R. J. Xue, Y. Z. Li, W. H. Wang, and H. Y. Bai, Revealing localized plastic flow in apparent elastic region before yielding in metallic glasses, *J. Appl. Phys.* **118**, 244901 (2015).
- [13] A. L. Greer, and Y. H. Sun, Stored energy in metallic glasses due to strains within the elastic limit, *Philos. Mag.* **96**, 1643 (2016).
- [14] M. Zhang, Y. M. Wang, F. X. Li, S. Q. Jiang, M. Z. Li and L. Liu, Mechanical relaxation-to-rejuvenation transition in a Zr-based bulk metallic glass, *Sci. Rep.* **7**, 625 (2017).
- [15] J. Pan, Y. X. Wang, Q. Guo, D. Zhang, A. L. Greer, and Y. Li, Extreme rejuvenation and softening in a bulk metallic glass, *Nat. Commun.* **9**, 560 (2018).
- [16] M. Samavatian, R. Gholamipour, A. A. Amadeh, and S. Mirdamadi, Role of tensile elastostatic loading on atomic structure and mechanical properties of  $\text{Zr}_{55}\text{Cu}_{30}\text{Ni}_5\text{Al}_{10}$  bulk metallic glass, *Mater. Sci. Eng. A* **753**, 218 (2019).
- [17] I. Regev, J. Weber, C. Reichhardt, K. A. Dahmen, and T. Lookman, Reversibility and criticality in amorphous solids, *Nat. Commun.* **6**, 8805 (2015).
- [18] N. V. Priezjev, Reversible plastic events during oscillatory deformation of amorphous solids, *Phys. Rev. E* **93**, 013001 (2016).
- [19] N. V. Priezjev, Nonaffine rearrangements of atoms in deformed and quiescent binary glasses, *Phys. Rev. E* **94**, 023004 (2016).
- [20] P. Leishangthem, A. D. S. Parmar, and S. Sastry, The yielding transition in amorphous solids

- under oscillatory shear deformation, *Nat. Commun.* **8**, 14653 (2017).
- [21] N. V. Priezjev, Collective nonaffine displacements in amorphous materials during large-amplitude oscillatory shear, *Phys. Rev. E* **95**, 023002 (2017).
- [22] N. V. Priezjev, Molecular dynamics simulations of the mechanical annealing process in metallic glasses: Effects of strain amplitude and temperature, *J. Non-Cryst. Solids* **479**, 42 (2018).
- [23] N. V. Priezjev, The yielding transition in periodically sheared binary glasses at finite temperature, *Comput. Mater. Sci.* **150**, 162 (2018).
- [24] I. Regev and T. Lookman, Critical diffusivity in the reversibility–irreversibility transition of amorphous solids under oscillatory shear, *J. Phys. Condens. Matter* **31**, 045101 (2018).
- [25] A. D. S. Parmar, S. Kumar, and S. Sastry, Strain localization above the yielding point in cyclically deformed glasses, *Phys. Rev. X* **9**, 021018 (2019).
- [26] P. Cao, M. P. Short, and S. Yip, Understanding the mechanisms of amorphous creep through molecular simulation, *PNAS* **114**, 13631 (2017).
- [27] Y. C. Lo, H. S. Chou, Y. T. Cheng, J. C. Huang, J. R. Morris, P. K. Liaw, Structural relaxation and self-repair behavior in nano-scaled Zr-Cu metallic glass under cyclic loading: Molecular dynamics simulations, *Intermetallics* **18**, 954 (2010).
- [28] N. V. Priezjev, Slow relaxation dynamics in binary glasses during stress-controlled, tension-compression cyclic loading, *Comput. Mater. Sci.* **153**, 235 (2018).
- [29] N. V. Priezjev, The effect of cryogenic thermal cycling on aging, rejuvenation, and mechanical properties of metallic glasses, *J. Non-Cryst. Solids* **503-504**, 131 (2019).
- [30] Q.-L. Liu and N. V. Priezjev, The influence of complex thermal treatment on mechanical properties of amorphous materials, *Comput. Mater. Sci.* **161**, 93 (2019).
- [31] M. Utz, P. G. Debenedetti, and F. H. Stillinger, Atomistic simulation of aging and rejuvenation in glasses, *Phys. Rev. Lett.* **84**, 1471 (2000).
- [32] D. J. Lacks and M. J. Osborne, Energy landscape picture of overaging and rejuvenation in a sheared glass, *Phys. Rev. Lett.* **93**, 255501 (2004).
- [33] W. Kob and H. C. Andersen, Testing mode-coupling theory for a supercooled binary Lennard-Jones mixture: The van Hove correlation function, *Phys. Rev. E* **51**, 4626 (1995).
- [34] T. A. Weber and F. H. Stillinger, Local order and structural transitions in amorphous metal-metalloid alloys, *Phys. Rev. B* **31**, 1954 (1985).
- [35] S. J. Plimpton, Fast parallel algorithms for short-range molecular dynamics, *J. Comp. Phys.*

- 117**, 1 (1995).
- [36] M. P. Allen and D. J. Tildesley, *Computer Simulation of Liquids* (Clarendon, Oxford, 1987).
- [37] A. Barbot, M. Lerbinger, A. Hernandez-Garcia, R. Garcia-Garcia, M. L. Falk, D. Vandembroucq, and S. Patinet, Local yield stress statistics in model amorphous solids, *Phys. Rev. E* **97**, 033001 (2018).
- [38] M. L. Falk and J. S. Langer, Dynamics of viscoplastic deformation in amorphous solids, *Phys. Rev. E* **57**, 7192 (1998).
- [39] K. Vollmayr, W. Kob, and K. Binder, How do the properties of a glass depend on the cooling rate? A computer simulation study of a Lennard-Jones system, *J. Chem. Phys.* **105**, 4714 (1996).
- [40] F. Varnik, L. Bocquet, and J.-L. Barrat, A study of the static yield stress in a binary Lennard-Jones glass, *J. Chem. Phys.* **120**, 2788 (2004).
- [41] J. Rottler and M. O. Robbins, Unified description of aging and rate effects in yield of glassy solids, *Phys. Rev. Lett.* **95**, 225504 (2005).

## Figures

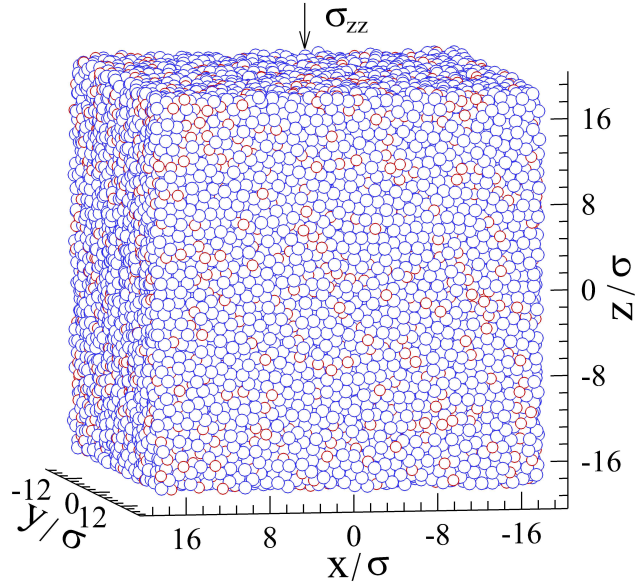


FIG. 1: (Color online) The spatial configuration of LJ atoms after cooling from  $T_{LJ} = 1.0 \varepsilon/k_B$  to  $0.01 \varepsilon/k_B$  with the rate  $10^{-5} \varepsilon/k_B \tau$  at zero pressure. The total number of atoms is 60 000. Note that atoms of types  $A$  and  $B$  are indicated by large blue and small red spheres, respectively. During elastostatic loading, the normal stress  $\sigma_{zz}$  is applied along the  $\hat{z}$  direction, while stresses  $\sigma_{xx}$  and  $\sigma_{yy}$  are set to zero.

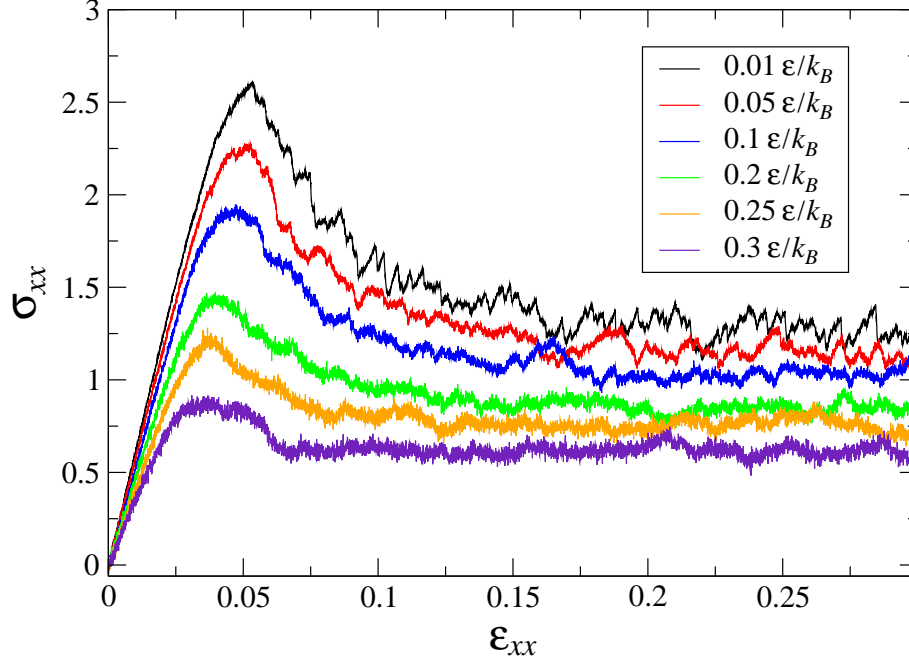


FIG. 2: (Color online) The dependence of stress (in units of  $\varepsilon\sigma^{-3}$ ) as a function of strain,  $\varepsilon_{xx}$ , during compression along the  $\hat{x}$  direction with the rate  $\dot{\varepsilon}_{xx} = 10^{-5} \tau^{-1}$  at temperatures  $T_{LJ} = 0.01 \varepsilon/k_B$  (black),  $0.05 \varepsilon/k_B$  (red),  $0.1 \varepsilon/k_B$  (blue),  $0.2 \varepsilon/k_B$  (green),  $0.25 \varepsilon/k_B$  (orange), and  $0.3 \varepsilon/k_B$  (indigo). The strain was imposed after the sample was cooled below the glass transition temperature with the rate  $10^{-5} \varepsilon/k_B \tau$  at zero pressure.

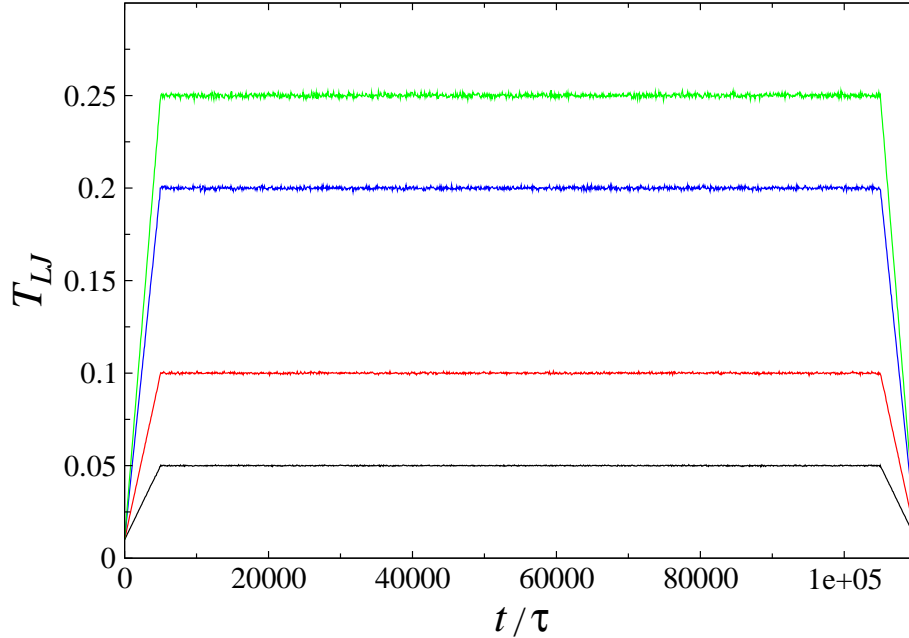


FIG. 3: (Color online) The temperature profiles during the loading protocols, which include a gradual heating during  $5000\tau$  from  $T_{LJ} = 0.01\epsilon/k_B$  to the annealing temperature,  $T_a$ , followed by the annealing period  $t_a = 10^5\tau$ , and a subsequent cooling to the reference temperature  $T_{LJ} = 0.01\epsilon/k_B$  during  $5000\tau$ . The values of the annealing temperature are  $T_a = 0.05\epsilon/k_B$  (black),  $0.1\epsilon/k_B$  (red),  $0.2\epsilon/k_B$  (blue), and  $0.25\epsilon/k_B$  (green).



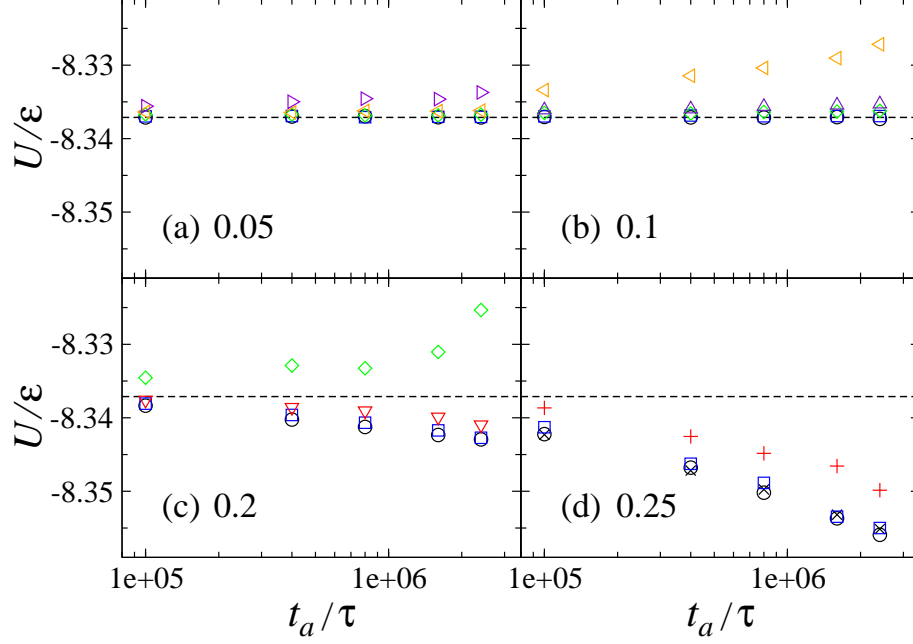


FIG. 4: (Color online) The potential energy as a function of the annealing time,  $t_a/\tau$ , for static stresses  $\sigma_{zz} = 0.0$  ( $\circ$ ),  $0.3 \varepsilon \sigma^{-3}$  ( $\times$ ),  $0.5 \varepsilon \sigma^{-3}$  ( $\square$ ),  $0.7 \varepsilon \sigma^{-3}$  ( $+$ ),  $0.8 \varepsilon \sigma^{-3}$  ( $\nabla$ ),  $1.0 \varepsilon \sigma^{-3}$  ( $\diamond$ ),  $1.2 \varepsilon \sigma^{-3}$  ( $\triangle$ ),  $1.5 \varepsilon \sigma^{-3}$  ( $\triangleleft$ ), and  $1.8 \varepsilon \sigma^{-3}$  ( $\triangleright$ ). The annealing temperatures are (a)  $T_a = 0.05 \varepsilon/k_B$ , (b)  $0.1 \varepsilon/k_B$ , (c)  $0.2 \varepsilon/k_B$ , and (d)  $0.25 \varepsilon/k_B$ . The horizontal dashed lines denote the potential energy level  $U = -8.337 \varepsilon$  at  $T_{LJ} = 0.01 \varepsilon/k_B$  and  $P = 0$  before the thermomechanical processing.

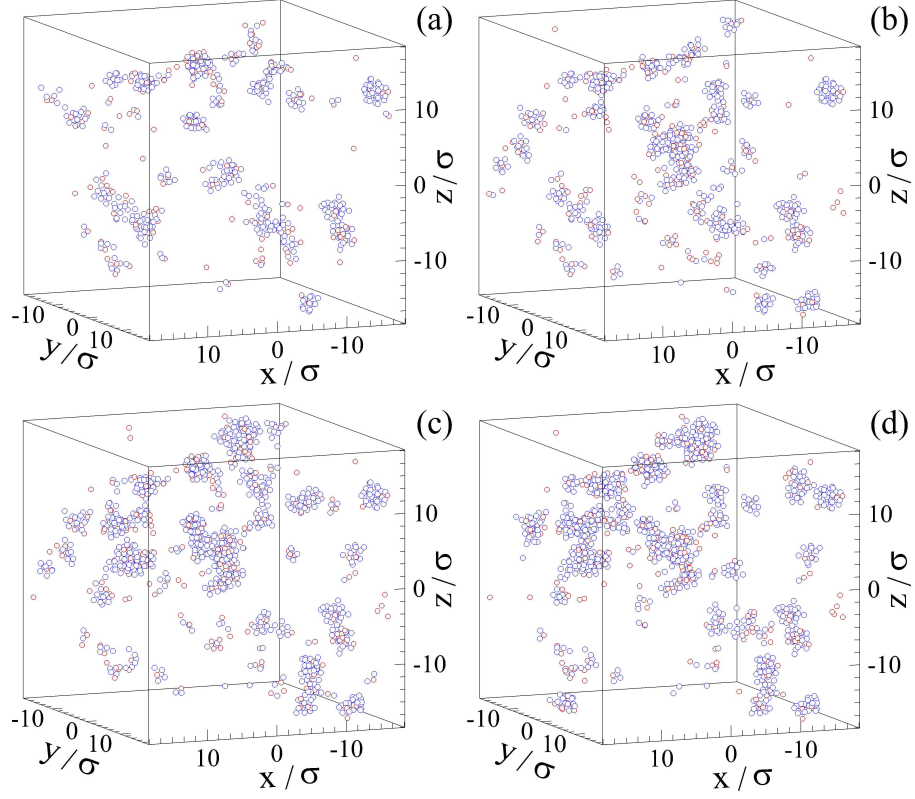


FIG. 5: (Color online) The snapshots of atoms with the nonaffine measure: (a)  $D^2(0, 10^5\tau) > 0.04\sigma^2$ , (b)  $D^2(0, 4 \times 10^5\tau) > 0.04\sigma^2$ , (c)  $D^2(0, 1.6 \times 10^6\tau) > 0.04\sigma^2$ , and (d)  $D^2(0, 2.4 \times 10^6\tau) > 0.04\sigma^2$ . The sample was kept at the temperature  $T_a = 0.1 \varepsilon/k_B$  and the static stress  $\sigma_{zz} = 0.5 \varepsilon\sigma^{-3}$ .

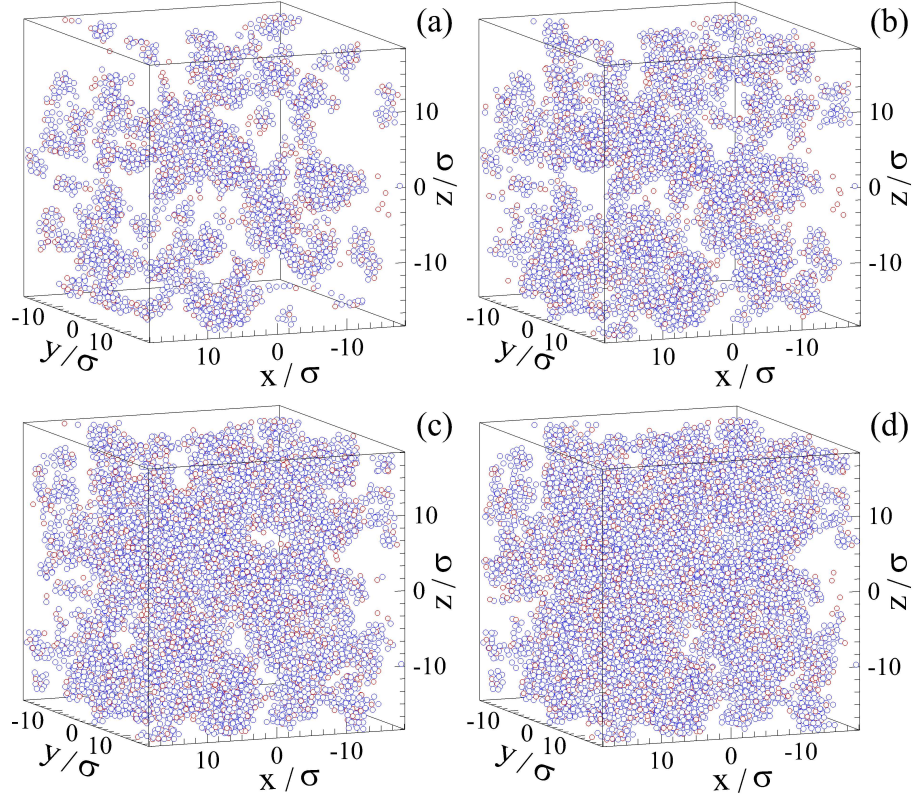


FIG. 6: (Color online) The positions of atoms with large nonaffine measure: (a)  $D^2(0, 10^5\tau) > 0.04\sigma^2$ , (b)  $D^2(0, 4 \times 10^5\tau) > 0.04\sigma^2$ , (c)  $D^2(0, 1.6 \times 10^6\tau) > 0.04\sigma^2$ , and (d)  $D^2(0, 2.4 \times 10^6\tau) > 0.04\sigma^2$ . The annealing temperature is  $T_a = 0.1 \varepsilon/k_B$  and the static stress is  $\sigma_{zz} = 1.5 \varepsilon\sigma^{-3}$ .

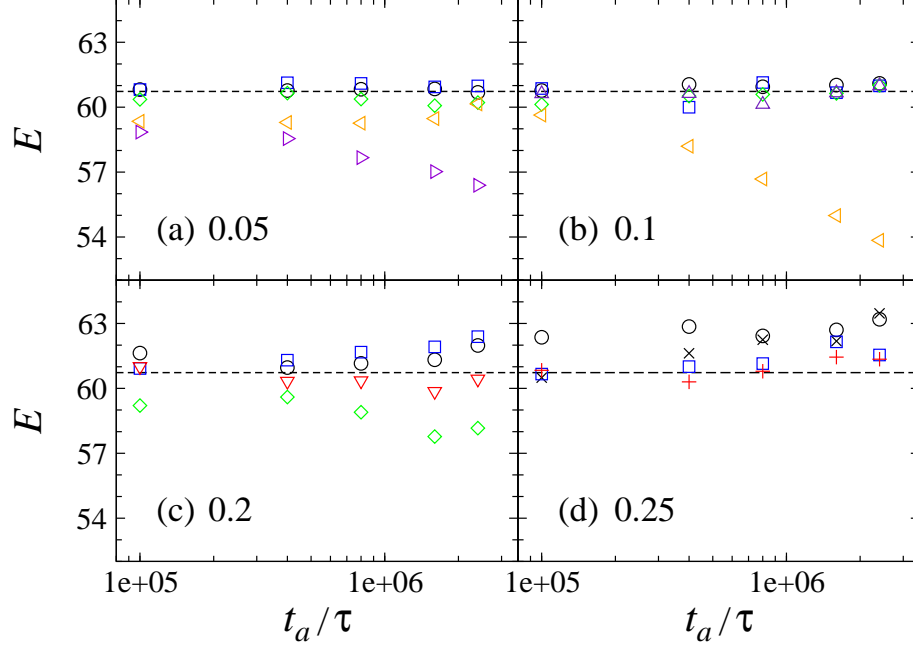


FIG. 7: (Color online) The elastic modulus  $E$  (in units of  $\epsilon\sigma^{-3}$ ) versus the annealing time,  $t_a$ , and temperatures (a)  $T_a = 0.05 \epsilon/k_B$ , (b)  $0.1 \epsilon/k_B$ , (c)  $0.2 \epsilon/k_B$ , and (d)  $0.25 \epsilon/k_B$ . The black dashed lines indicate the value of the elastic modulus  $E = 60.73 \epsilon\sigma^{-3}$  before the elastostatic loading. The static stress is  $\sigma_{zz} = 0.0$  ( $\circ$ ),  $0.3 \epsilon\sigma^{-3}$  ( $\times$ ),  $0.5 \epsilon\sigma^{-3}$  ( $\square$ ),  $0.7 \epsilon\sigma^{-3}$  ( $+$ ),  $0.8 \epsilon\sigma^{-3}$  ( $\nabla$ ),  $1.0 \epsilon\sigma^{-3}$  ( $\diamond$ ),  $1.2 \epsilon\sigma^{-3}$  ( $\triangle$ ),  $1.5 \epsilon\sigma^{-3}$  ( $\triangleleft$ ), and  $1.8 \epsilon\sigma^{-3}$  ( $\triangleright$ ).

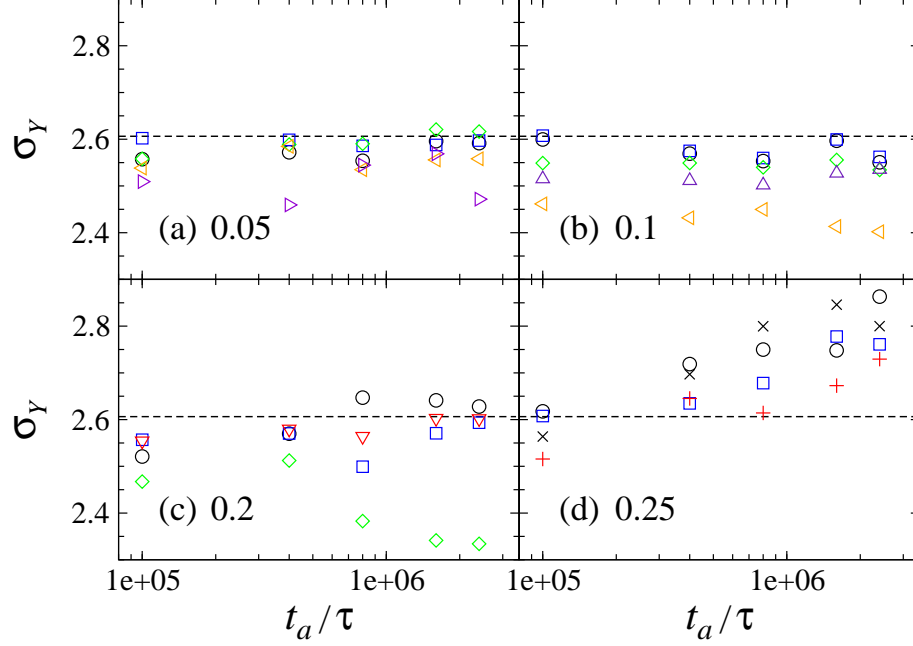


FIG. 8: (Color online) The yielding peak  $\sigma_Y$  (in units of  $\varepsilon\sigma^{-3}$ ) as a function of the annealing time and temperatures (a)  $T_a = 0.05\varepsilon/k_B$ , (b)  $0.1\varepsilon/k_B$ , (c)  $0.2\varepsilon/k_B$ , and (d)  $0.25\varepsilon/k_B$ . The horizontal lines mark the value  $\sigma_Y = 2.61\varepsilon\sigma^{-3}$  before the thermal loading. The applied stress is  $\sigma_{zz} = 0.0$  (o),  $0.3\varepsilon\sigma^{-3}$  (x),  $0.5\varepsilon\sigma^{-3}$  (□),  $0.7\varepsilon\sigma^{-3}$  (+),  $0.8\varepsilon\sigma^{-3}$  (▽),  $1.0\varepsilon\sigma^{-3}$  (◇),  $1.2\varepsilon\sigma^{-3}$  (△),  $1.5\varepsilon\sigma^{-3}$  (◁), and  $1.8\varepsilon\sigma^{-3}$  (▷).